



Download

Comparative study on computation of ship added resistance in waves

Min-Guk Seo, Dong-Min Park, Kyung-Kyu Yang, Yonghwan Kim

Show more

Outline | Share | Cite

<https://doi.org/10.1016/j.oceaneng.2013.07.008>

Get rights and content

Highlights

- Three different numerical methods are compared for added resistance computation.
- Both the far-field and near-field formulations are applied.
- Asymptotic formulae are compared in short waves.
- Comparisons are made for different numerical schemes and formulations.

Abstract

Recently, the design of commercial ships that produce less greenhouse gas has been of great interest in naval architecture fields. Ship designers are asked to find optimum hull forms with minimum resistance in ocean waves. An accurate computation of added resistance, therefore, is getting more important for the prediction of power increase in random ocean waves. This study focuses on a comparison of the computational results of added resistance on ships in waves. To calculate added resistance, three different numerical approaches are applied: the strip method, the Rankine panel method, and the Cartesian grid method, which solves the Euler equation. In order to predict added resistance, near- and far-field approaches are adopted in the strip and Rankine panel methods, while added resistance is calculated directly in the Cartesian grid method. The computational results are validated by comparing them with experimental data on Wigley hulls, Series 60 hulls, and the S175 containership, and show reasonable agreements for all models. The study is extended to the analysis of added resistance in short wavelengths; therefore, the established asymptotic methods for short waves are examined.

Previous

Next

Keywords

Added resistance; EEDI; Rankine panel method; Strip method; Cartesian-grid method; Short-wave approximation

1. Introduction

When a ship navigates in a seaway, the ship's forward speed decreases, compared to that in calm sea, because of added resistance due to winds, waves, rudder angle, and so forth. The magnitude of added resistance is about 15–30% of calm-water resistance. An accurate prediction of added resistance, therefore, is important in the propulsion power design of a ship. Moreover, in recent years, discussions at the International Maritime Organization (IMO) have resulted in the development of an Energy Efficiency Design Index (EEDI) to measure how much greenhouse gas a ship emits, and to restrict greenhouse gas emissions from ships. For these reasons, ship designers should find optimum hull forms to minimize resistance in ocean waves, and pay more attention to the added resistance problem.

Added resistance due to waves is one of the major components that affect ship performance in actual seas. The added resistance problem due to waves, therefore, has been widely studied over a long time. There have been many researches to predict added resistance on ships by conducting experiments, and several results have been introduced. [Gerritsma and Beukelman \(1972\)](#) and [Storm-Tejsen et al. \(1973\)](#) measured added resistance on the Series 60 models. [Fuji and Takahashi \(1975\)](#) and [Nakamura and Naito \(1977\)](#) performed added resistance tests with the S175 containership. The added resistances on Wigley models were measured by [Journee \(1992\)](#).

Meanwhile, there are two major approaches that can be used to analyze the added resistance problem: the far-field and near-field methods. The far-field method, which is based on momentum conservation theory, was introduced by [Maruo \(1960\)](#). It was further elaborated by [Joozen \(1966\)](#), and by [Newman \(1967\)](#). Recently, [Kashiwagi et al. \(2009\)](#) used Maruo's approach to calculate added resistance by applying enhanced unified theory, and they introduced a practical factor for complementing the results of added resistance at short wavelengths. [Liu et al. \(2011\)](#) applied a hybrid time-domain Rankine source-Green function method to solve the basic seakeeping problem; then Maruo's approach was adopted for the calculation of added resistance. Another far-field method, based on the radiated energy approach, was proposed by [Gerritsma and Beukelman \(1972\)](#), which basically follows Maruo's approach. Later, [Salvesen \(1978\)](#) applied Gerritsma and Beukelman's method to analyze the added resistance problem, using basic results of the STF ([Salvesen et al., 1970](#)) strip method, and found quite satisfactory results for the ship hull forms investigated. Recently, [Fang and Chen \(2006\)](#) followed Salvesen's approach, but used a different strip theory to modify the method, obtaining some improved results. Generally, these far-field methods are simple and powerful, because there is no need to solve a complete boundary value problem to obtain the body pressure; thus the far-field method has been extensively used to estimate the added resistance in real applications. This method, however, has limitations in handling a proper control surface, and it is not easy to apply to a multi-body problem. Due to the significant development of computer power, the near-field method, which calculates added resistance by integrating the second-order pressure on a body surface, has been acclaimed. The near-field method makes it easy to understand physical phenomena, and to extend it to multi-body problems or nonlinear problems. Many researches have been conducted using this near-field method to estimate added resistance. [Faltinsen et al. \(1980\)](#) used the near-field approach, with good validation results. They also addressed the deficiency of this approach in short waves, and introduced a simplified asymptotic method to complement this deficiency. [Grue and Biberg \(1993\)](#) and [Ye and Hsiung \(1997\)](#) applied wave Green function to the added resistance problem. These efforts were mostly based on frequency-domain approaches.

Despite the success of previous studies on the added resistance problem, very limited researches can be found that are based on the Rankine panel method, which is widely applied today to the ship motion problem, including linear and nonlinear problems. [Joncquez et al. \(2008\)](#) analyzed the added resistance problem by extending a ship motion program, AEGIR, which is based on a higher-order Rankine panel method, and they applied both the far- and near-field methods. A comparison between the computational results based on Neumann-Kelvin and double-body linearization schemes was also carried out by [Joncquez \(2009\)](#). [Kim and Kim \(2011\)](#) and [Kim et al. \(2012\)](#) also applied the higher-order Rankine panel method to the added resistance problem using the far- and near-field methods. An analysis of added resistance in irregular waves was carried out, and the proper criteria of time window and number of wave frequencies were suggested for irregular waves.

Added resistance in short wavelength is another main concern in this area, because it is difficult to calculate added resistance accurately using the previous calculation methods. In general, "short wavelength" means that the wavelength over the ship length is smaller than 0.5 ($\lambda/L < 0.5$). In short waves, incident waves are mostly reflected and ship motion is not large. Therefore, diffraction component near the ship bow plays a key role in added resistance. This may increase nonlinear effects, which are not considered in the prescribed methods, resulting in some discrepancy between numerical results and experimental data in short wavelength. To complement this problem, a few researches were carried out. [Fuji and Takahashi \(1975\)](#) derived a semi-empirical formula of added resistance in short waves, by adopting some complement coefficients to the drift force formula of a fixed vertical cylinder. [Faltinsen et al. \(1980\)](#) also derived asymptotic formula of added resistance in short waves, by assuming that the ship has a vertical side at the water plane, and the wavelength is small compared to the draft of the ship. These two approaches give good results for relatively blunt bodies; however, some poor results can be obtained for fine hulls, such as containerships. In order to improve this drawback, [Kuroda et al. \(2008\)](#) proposed an improved expression that was based on

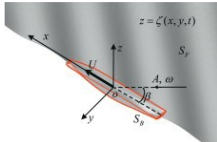
Fujii and Takahashi's method. They modified compliment coefficients, using experimental data.

Recently, thanks to the rapid development of computer power, computational fluid dynamics (CFD) has been applied to some seakeeping problems. Most of them, however, focused on the ship motion problem, and there are few research works on the added resistance problem. Orihara and Miyata (2003) solved ship motions in regular head wave conditions, and evaluated added resistance of a SR-10S containership (typically known as S175 containership) in waves, using a CFD simulation method called WISDAM-X. The Reynolds-averaged Navier-Stokes (RANS) equation was solved using a finite-volume method with an overlapping grid system. In a recent comparative study on seakeeping computation tools (Bunnik et al., 2010), two groups (ECN and Kyushu University) calculated the added resistance of a containership in head seas. ECN used their CFD code "ISIS", which is based on an unstructured finite-volume RANS method, with an analytical weighting mesh deformation approach, to treat the moving body problem. The constrained interpolation profile (CIP)-based Cartesian grid method was applied as a flow solver in a program called "RIAM-CMEN" developed by Hu and Kashiwagi (2007).

In the present study, a frequency-domain strip method and a time-domain Rankine panel method are applied to solve the seakeeping problem, and to calculate the first-order potential and linear ship responses, as a necessity for the added resistance calculation. Both the near-field and far-field methods are adopted for the calculation of added resistances on ships. The Cartesian grid method, which solves the Euler equation directly, is also applied to estimate added resistance. In this method, the wave-body interaction problem is considered as a multiphase problem, and volume fraction functions are defined, in order to distinguish each phase in a Cartesian grid system. The added resistance is calculated by subtracting the steady surge force from the mean surge force measured in motion problems. Computational results are validated for several models, including Wigley hulls, Series 60 hulls ($C_D=0.7, 0.8$) and the S175 containership, by comparing them with experimental data. In addition, to complement the results of added resistance in short wavelengths, the established asymptotic methods are examined.

2. Mathematical background for ship motion analysis

Consider a ship advancing with a certain forward speed, U , in the presence of incident waves. In this study, the ship motion problem is solved by using three different methods: the frequency-domain strip method, the time-domain Rankine panel method, and the Cartesian grid method. To this end, let us define a ship-fixed coordinate system, as in Fig. 1. Here, A , ω and β represent the incident wave amplitude, frequency and heading angle, respectively. S_B and S_F denote the body surface and the free-surface, respectively.



[Download : Download full-size image](#)

Fig. 1. Coordinate system for the ship motion problem.

2.1. The strip method in the frequency domain

If a slender body is in low forward speed and high incident wave frequency conditions, hydrodynamic coefficients can be obtained by integrating the sectional solutions. For a two-dimensional strip as shown in Fig. 2(a), the velocity potential ϕ satisfies the following boundary value problem

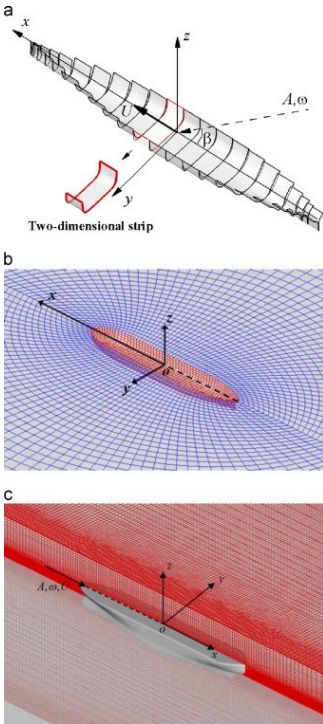
$$\nabla^2 \phi_k = 0, \quad (k = 2, 3, 4) \quad \text{in fluid domain} \quad (1)$$

$$-\omega_e^2 \phi_k + g \frac{\partial \phi_k}{\partial z} = 0, \quad (k = 2, 3, 4) \quad \text{on } z = 0 \quad (2)$$

$$\frac{\partial \phi_k}{\partial n} = V_{01}, \quad (k = 2, 3, 4) \quad \text{on } S_0 \quad (3)$$

$$\lim_{y \rightarrow \infty} \nabla \phi_k = 0, \quad (k = 2, 3, 4) \quad (4)$$

where, $k=2$ for sway motion, $k=3$ for heave motion, and $k=4$ for roll motion. ω_e and g refer to an encounter wave frequency and gravity constant, respectively.



[Download : Download full-size image](#)

Fig. 2. Example meshes for three numerical methods (a) Strip method, (b) Rankine panel method and (c) Cartesian grid method.

To implement numerical computation of the wave Green function, a computer code developed by Scavounos (1985), NIIRID, is adopted. Using this program, sectional hydrodynamic coefficients and exciting forces can be calculated. In calculation of the motion, to compute the total hydrodynamic coefficients, STF (Salvesen, Tack and Faltinsen) strip theory (1970) is used. Since this theory is well known, the details are not described here.

If the ship is symmetric about its center-plane, the heave and pitch motion can be decoupled from the sway, roll, and yaw motion. The heave – pitch coupled equation in the frequency domain is expressed as follows:

$$\sum_{k=-\infty}^{\infty} [(M_{jk} + A_{jk})\ddot{\xi}_k + B_{jk}\dot{\xi}_k + C_{jk}\xi_k] = F_j e^{j\omega t}, \quad \text{for } j = 3 \text{ and } 5 \quad (5)$$

where M_{jk} is the mass matrix, A_{jk} and B_{jk} are added-mass and damping coefficients, C_{jk} is the hydrostatic restoring coefficient and F_j is the complex amplitudes of the exciting force and moment. These hydrodynamic coefficients and exciting forces can be obtained from the summation of 2D sectional added-mass, damping coefficient, and excitation force.

2.2. The Rankine panel method in the time domain

When the ship is assumed to be a rigid-body, the wave-induced body motion can be written as follows:

$$\vec{\delta}(\vec{x}, t) = \vec{\xi}_T(t) + \vec{\zeta}_R(t) \times \vec{x} \quad (6)$$

where, $\vec{\xi}_T = (\xi_1, \xi_2, \xi_3)$ and $\vec{\zeta}_R = (\xi_4, \xi_5, \xi_6)$ are the translation and rotation ship motions, respectively.

Adopting the velocity potential ϕ in the fluid domain, and decomposing the total velocity potential and total wave elevation to basis, incident, and disturbed components, the linearized boundary conditions can be considered

$$\frac{\partial \phi}{\partial n} - (\vec{U} \cdot \nabla \Phi) \cdot \nabla \zeta_d = \frac{\partial \phi}{\partial z} \zeta_d + \frac{\partial \phi}{\partial z} + (\vec{U} \cdot \nabla \Phi) \cdot \nabla \zeta_d \quad \text{on } z = 0 \quad (7)$$

$$\frac{\partial \phi}{\partial n} - (\vec{U} \cdot \nabla \Phi) \cdot \nabla \phi_d = -\frac{\partial \phi}{\partial z} - g \zeta_d + \left[\vec{U} \cdot \nabla \Phi - \frac{1}{2} \nabla \Phi \cdot \nabla \Phi \right] + (\vec{U} \cdot \nabla \Phi) \quad \text{on } z = 0 \quad (8)$$

$$\begin{aligned} \frac{\partial \phi}{\partial z} &= \sum_{j=1}^J \left(\frac{\partial \phi}{\partial z} n_j + \xi_j m_j \right) - \frac{\partial \phi}{\partial z} \\ \text{on } \Sigma_B(m_1, m_2, m_3) &= (\vec{n} \cdot \nabla)(\vec{U} \cdot \nabla \Phi)(m_1, m_2, m_3) \\ &= (\vec{n} \cdot \nabla)(\vec{x}) \times (\vec{U} \cdot \nabla \Phi) \end{aligned} \quad (9)$$

where, Φ indicates the basis potential and its order is $O(1)$. ϕ_I and ζ_d denote the incident wave potential and elevation, respectively. Similarly, ϕ_d and ζ_d represent the disturbed wave potential and elevation. Both incident and disturbed components are $O(\epsilon)$. The basis potential takes uniform-flow, $-Ux$, in the Neumann–Kelvin linearization, while it takes double-body flow potential in the double-body linearization. m_j is the m-term, which includes the effects of interaction between the steady and unsteady solutions (Nakos, 1990).

The ship motion can be obtained by solving an equation of motion, as follows:

$$[M]\{\vec{\xi}\} = \{F_{F.K.}\} + \{F_{Res.}\} + \{F_{H.D.}\} \quad (10)$$

where, $[M]$ is the mass matrix of the ship, and $\{F_{F.K.}\}$ and $\{F_{Res.}\}$ are the Froude–Krylov force and restoring force, respectively. In the linear equation of motion, a constant restoring coefficient and a linear Froude–Krylov force are applied, under the assumption that the ship motion and wave amplitude are small. $\{F_{H.D.}\}$ represents the hydrodynamic force due to the radiation and diffraction waves of a ship, except for the Froude–Krylov and restoring force.

To solve the prescribed linear boundary value problem, Green's second identity is applied, by discretizing the boundary surface, as shown in Fig. 2(b). The Rankine source ($G=1/\rho$) that only satisfies the Laplace equation is distributed to the discretized body surface and free-surface; then the 2nd Green's identity can be expressed as follows:

$$\phi_d + \iint_{S_B} \phi_d \frac{\partial G}{\partial n} dS - \iint_{S_B} \frac{\partial \phi_d}{\partial n} G dS = \iint_{S_B} \phi_d \frac{\partial G}{\partial n} dS - \iint_{S_B} \phi_d \frac{\partial G}{\partial n} dS \quad (11)$$

In the present study, the velocity potential, wave elevation and normal flux along the fluid boundary are approximated using the B-spline basis function.

$$\phi_j(\vec{x}, t) = \sum_{j=1}^J (\phi_{d,j}(t) B_j(\vec{x}) \zeta_d(\vec{x}, t) + \sum_{j=1}^J (\zeta_{d,j}(t) B_j(\vec{x}) \frac{\partial \phi_d}{\partial z}(\vec{x}, t)) \quad (12)$$

$B_j(\vec{x})$ is a B-spline basis function, and $(\phi_{d,j}(t), \zeta_{d,j}(t))$ and $(\delta\phi_d, \delta\zeta_d)$ denote the coefficients of velocity potential, wave elevation and the normal flux at the j-th discretized boundary panel, respectively. The radiation condition is satisfied by adopting the concept of an artificial wave-absorbing zone. An artificial wave-absorbing zone is distributed around the truncated boundary of the free-surface, and the kinematic free-surface boundary condition is modified to include an artificial damping mechanism. Details of numerical implementations are found in Kim et al., 2010, Kim et al., 2012.

2.3. The Cartesian grid method

2.3.1. Flow solver

The governing equations for incompressible and inviscid fluid flow are the continuity and Euler equations, which are written in their conservative forms as follows:

$$\int_{\Gamma} (\vec{u} \cdot \vec{n}) dS = 0 \quad (13)$$

$$\frac{\partial}{\partial t} \int_{\Omega} \vec{u} \cdot dV + \int_{\Gamma} \vec{u} \cdot (\vec{u} \cdot \vec{n}) dS = \frac{1}{\rho} \left[- \int_{\Gamma} p \vec{n} \cdot dS + \int_{\Gamma} \vec{f} \cdot \vec{n} dV \right] \quad (14)$$

where, Ω indicates a control volume, and Γ means the control surface enclosing the control volume. \vec{n} is a unit outward normal vector on Γ , ρ is the fluid density, and p and \vec{u} denote the pressure and velocity vector, respectively. In addition, \vec{f} indicates the body force vector.

Velocity and pressure are coupled by a fractional step method, involving a solving procedure that is divided into three steps, one advection and two non-advection phases, as follows:

$$\frac{\int_{\Gamma} \vec{u}^* \cdot \vec{n} - \vec{u}^* \cdot \vec{n}}{\Delta t} + \int_{\Gamma} \vec{u}^* \cdot (\vec{u}^{**} \cdot \vec{n}) dS = 0 \quad (15)$$

$$\frac{\int_{\Gamma} \vec{u}^* \cdot \vec{n} - \vec{u}^* \cdot \vec{n}}{\Delta t} = \frac{1}{\rho \Delta t} \int_{\Omega} \vec{f} \cdot dV \quad (16)$$

$$\frac{\int_{\Gamma} \vec{u}^{**} \cdot \vec{n} - \int_{\Gamma} \vec{u}^{**} \cdot \vec{n}}{\Delta t} = -\frac{1}{\rho \Delta t} \int_{\Omega} p^{p+1} \vec{n} dS \quad (17)$$

Superscripts (*, **, n , $n+1$) indicate intermediate values during time advancement. The pressure field is calculated through solving the pressure Poisson equation, which is obtained by taking the divergence of Eq. (17), and using the continuity equation and the divergence theorem.

$$\nabla \left(\frac{1}{\rho \Delta t} \int_{\Omega} p^{p+1} \vec{n} dS \right) = \frac{1}{\Delta t} \int_{\Gamma} \vec{u}^{**} \cdot \vec{n} dS \quad (18)$$

Spatial discretization is carried out based on the finite volume approach with staggered variable allocation. The surface integration is approximated by using a midpoint rule, and the cell center value for the convective term is interpolated with a monotonized central (MC) limiter function (Waterson and Deconinck, 2007). A directional splitting approach is applied in order to consider multidimensional effects, and other spatial discretization is conducted based on the second-order central difference scheme.

The free surface is determined by an interface capturing method. To identify the different phases in the multi-phase flow, density functions, γ_m are defined for liquid ($m=1$), gas ($m=2$) and solid body ($m=3$). The density function for the liquid phase is calculated by solving the following advection equation:

$$\frac{\partial \gamma_l}{\partial t} + \vec{u} \cdot \nabla \gamma_l = 0 \quad (19)$$

To solve this advection equation, various numerical methods have been proposed in the literature. Among them, the tangent of hyperbola for interface capturing (THINC) scheme introduced by Xiao et al. (2005) is used in the present computation. The basic idea of the THINC method is that the density function profile inside of a computational cell is approximated as a hyperbolic tangent function, to reproduce the jump of density function near the free surface. Yokoi (2007) developed an improved multi-dimensional THINC scheme by adapting the weighed line interface calculation (WLIC) method, which takes into account the information of the surface normal vector, while maintaining a simple implementation. The THINC method combined with the WLIC method is used throughout the computation.

2.3.2. Treatment of complex geometry

An arbitrary body is embedded in a Cartesian-grid system, and identified by a volume fraction function of the solid body, as shown in Fig. 2(c). To calculate the volume fraction of the solid body in each cell, a level-set-based method is applied. The first step of calculating the signed distance field is to read the geometric information of a solid body, represented by a triangular surface mesh. For grid points near each triangular surface, the distance field is calculated by transformation of the given triangle to a unit right triangle, and defining the quadratic distance function, which has minimum value when the gradient of the quadratic function equals zero. When the minimum value is located inside the transformed triangle, inverse transformation gives the coordinates of the closest point corresponding to a grid point. Otherwise, the intersection point of a triangle edge or vertex with contour line should be obtained. The detailed procedure is well explained in Eberly (2008).

To complete the calculation of volume fraction, determination of whether the grid point is inside or outside of the body should be performed. This is done by checking the sign of the inner product of the outward normal vector, and the direction vector between the grid point and the corresponding closest point. When the closest point is located at a triangle edge or vertex, another definition of normal vector is needed. The angle-weighted pseudo-normal vector introduced by Barentzen and Aanen (2005) is used in this study, which is defined at each triangle vertex and edge. After obtaining the signed distance field from the triangular surface for each grid point, the volume fraction function can be calculated by using a smoothed Heaviside function.

$$H_\alpha(\psi) = \begin{cases} 0 & \text{if } \psi < -\alpha \\ \frac{1}{2} \left[1 + \frac{\psi}{\alpha} + \frac{1}{2} \sin \left(\frac{\pi \psi}{2\alpha} \right) \right] & \text{if } |\psi| \leq \alpha \\ 1 & \text{if } \psi > \alpha \end{cases} \quad (20)$$

where, ψ is a signed distance function, and α is a smoothing length, which is fixed as half of the diagonal distance of the smallest cell in this study.

To impose a no-slip boundary condition on the ship surface, a volume-weighted formulation is used.

$$\tilde{\vec{u}} = \vec{u} (1 - \eta_1^2) + \vec{U}_{body} \eta_1^2$$

where, $\tilde{\vec{u}}$ is the corrected velocity, \vec{U}_{body} is the body velocity and η_1^2 is the volume fraction of the body in the corresponding control volume. After solving the fluid part, the hydrodynamic force and moment acting on the body are calculated from the volume integral formula (Hu and Kashiwagi, 2004).

$$\vec{F} = - \iiint_V \nabla p \gamma_1 dV \quad (21)$$

$$\vec{M} = - \iiint_V (\vec{x} - \vec{x}_{cg}) \times \nabla p \gamma_1 dV \quad (22)$$

where, V indicates the whole domain volume, and \vec{x}_{cg} denotes the center of gravity coordinate vector.

3. Prediction of added resistance

To compute the added resistance on ships, both the far- and near-field methods are applied. The far-field method calculates the added resistance by considering the change of the second-order momentum far enough away from the body, and the near-field method calculates by integrating the second-order pressure on the body surface. In the case of the Cartesian grid method, the added resistance is calculated by integrating the pressure on the body surface, and subtracting the steady surge force from the mean surge force in waves.

3.1. The strip method

3.1.1. The near-field method (direct pressure integration method)

The near-field method based on direct pressure integration is applied to calculate the added resistance on ships. The added resistance can be obtained from the integration of pressure on the wetted surface, as follows:

$$R = \int_{\Omega} \left\{ -\frac{\partial \bar{p} \bar{c}^2}{\partial z} \right\} n_1 ds - \omega_m^2 M \zeta \bar{\xi}_3 + \omega_m^2 M \bar{f}_{\Omega_2} - \bar{z} \bar{\zeta}_3 \bar{K}_0 + \rho \int_{\Omega_2} \left[\begin{aligned} & (\zeta_3 - x \xi_3 - z \xi_1 \eta_1) \frac{\partial}{\partial y} \left(\frac{\partial \bar{p}}{\partial y} - U \frac{\partial \bar{u}}{\partial y} \right)_{\eta_1} \\ & + (\zeta_3 - x \xi_3 + z \xi_1 \eta_1) \frac{\partial}{\partial x} \left(\frac{\partial \bar{p}}{\partial x} - U \frac{\partial \bar{u}}{\partial x} \right)_{\eta_1} \\ & + \frac{1}{2} \left(\left(\frac{\partial u}{\partial x} \right)^2 + \left(\frac{\partial u}{\partial y} \right)^2 + \left(\frac{\partial u}{\partial z} \right)^2 \right) \end{aligned} \right] n_1 ds \quad (24)$$

where, $\zeta = \zeta_3 - x \eta_3 + y \eta_4$ is the relative wave amplitude along the ship, and the bar over the equations indicates the time-average value. The subscript, m , means the average position on the wetted section. Details of this formula are presented in Faltinsen et al. (1980).

3.1.2. The far-field method (momentum conservation method)

A momentum conservation method is proposed by Maruo (1960). If there is no work done by external forces, the formulation can be expressed as follows:

$$R = \frac{d\phi}{dt} \int_0^{2\pi} |H(\theta)|^2 (\cos \theta + \cos \beta) d\theta \quad (25)$$

where, k is the wave number, β is the incident wave angle, and $H(\theta)$ is the Kochin function, defined as

$$H(\theta) = \iint_{S_p} \left(\frac{\partial}{\partial n} \Phi - \Phi \frac{\partial}{\partial n} \right) e^{ikx - i\alpha \cos \theta - i\beta \sin \theta} \quad (26)$$

In order to reduce this equation to simpler form, a ship is assumed to be a slender body. This means that the ship's beam and draft are much smaller than the length of ship, and $\Phi \ll \delta \Phi / \delta n$ is satisfied. From these assumptions, Eq. (26) can be expressed as follows in the far field:

$$H(\theta) = \iint_{S_p} -\omega B(x) [A e^{-ikx \cos \theta} + i \xi_3 - i \xi_1] e^{-ks \cos \theta} ds \quad (27)$$

where, $B(x)$ is the beam of the ship's waterline, and ξ_3 and ξ_1 are the heave and pitch motion, respectively. Details of Eq. (27) are presented in Newman (1967).

3.1.3. The far-field method (radiated energy method)

As the other far-field method, Salvesen's formula uses the energy radiated from the ship to predict added resistance. Salvesen's formula is given by

$$R = -\frac{1}{2} k \cos \beta \sum_{j=3,5} \xi_j \left\{ (F_j^A)^* + F_j^D \right\} + R_f \quad (28)$$

where, ξ_j is the motion calculated by the strip theory, $(F_j^A)^*$ is the complex conjugate of the Froude-Krylov exciting force, and F_j^D is the diffraction force to the complex conjugate incident wave potential. R_f is given by

$$R_f = -\frac{1}{2} \zeta_1^2 \frac{d}{ds} k \cos \beta \int_L e^{-2kds} (b_{23} + b_{22} \sin^2 \beta) ds \quad (29)$$

where, ζ_1 is the incident wave amplitude, d is the sectional draft and s is the sectional-area coefficient. b_{23} and b_{22} are the sectional heave and sway damping coefficient, respectively. These coefficients can be obtained during the ship motion calculation. Details of this formula are presented in Salvesen (1978).

3.2. The Rankine panel method

3.2.1. The near-field method (direct pressure integration method)

By using Bernoulli's equation and Taylor's series expansion, the second-order pressure can be provided on the mean body surface, and the second-order force can be obtained by integrating the second-order pressure. The added resistance can be obtained by averaging the longitudinal component of the second-order force signal. The second-order force can be formulated as follows:

$$\begin{aligned} \vec{F}_2 &= f_{WZ} \frac{1}{2} \rho g (\zeta - (\xi_3 + \xi_1 y - \xi_2 x))^2 \cdot \vec{n} \cdot dL - \rho \int_{WZ} \vec{u} \\ &\quad \cdot \left((\vec{U} - \frac{1}{2} \nabla \Phi) \cdot \nabla \Phi \right) (\zeta - (\xi_3 + \xi_1 y - \xi_2 x)) \cdot \vec{n}_1 \cdot dL - \rho \int_{WZ} \vec{u} \\ &\quad \cdot \left(-(\vec{U} - \frac{1}{2} \nabla \Phi) \cdot \nabla \Phi \right) (\zeta - (\xi_3 + \xi_1 y - \xi_2 x)) \cdot \vec{n} \cdot dL - \rho \iint_{\overline{\Gamma}_2} y_2 \cdot \vec{n}_2 \cdot ds \\ &\quad f_{\overline{\Gamma}_2} \frac{1}{2} (\nabla (\phi_1 + \phi_2) \cdot \nabla (\phi_1 + \phi_2)) \cdot \vec{n} \cdot ds - \rho \\ &\quad \iint_{\overline{\Gamma}_2} \vec{\delta} \cdot \nabla \left(\frac{\partial \phi_1 + \phi_2}{\partial n} - (\vec{U} - \nabla \Phi) \cdot \nabla (\phi_1 + \phi_2) \right) \cdot \vec{n} \cdot ds - \rho \\ &\quad \iint_{\overline{\Gamma}_2} \left(g(\xi_3 + \xi_1 y - \xi_2 x) + \frac{\partial \phi_1 + \phi_2}{\partial n} - (\vec{U} - \nabla \Phi) \cdot \nabla (\phi_1 + \phi_2) \right) \times \vec{n}_1 \cdot ds - \rho \\ &\quad \iint_{\overline{\Gamma}_2} \left[\left(-(\vec{U} - \frac{1}{2} \nabla \Phi) \cdot \nabla \Phi \right) \cdot \vec{n}_1 \right] ds - \rho \iint_{\overline{\Gamma}_2} \vec{\delta} \cdot \nabla \left(-(\vec{U} - \frac{1}{2} \nabla \Phi) \cdot \nabla \Phi \right) \cdot \vec{n}_1 \cdot ds \quad (30) \end{aligned}$$

where, WZ and $\overline{\Gamma}_2$ represent the waterline and wetted surface of the mean body, respectively. \vec{n}_1 and \vec{n}_2 are the first- and second-order normal vectors, and are expressed as follows:

$$\begin{aligned} \vec{n}_1 &= \begin{bmatrix} 0 & -\xi_2 & \xi_1 \\ \xi_2 & 0 & -\xi_1 \\ -\xi_1 & \xi_1 & 0 \end{bmatrix} \begin{bmatrix} n_1 \\ n_2 \\ n_3 \end{bmatrix}, \vec{n}_2 \\ &= \frac{1}{2} \begin{bmatrix} -(\xi_1^2 + \xi_2^2) & 0 & 0 \\ 2\xi_1 \xi_2 & -(\xi_1^2 + \xi_2^2) & 0 \\ 2\xi_1 \xi_2 & 2\xi_2 \xi_3 & -(\xi_1^2 + \xi_2^2) \end{bmatrix} \begin{bmatrix} n_1 \\ n_2 \\ n_3 \end{bmatrix} \quad (31) \end{aligned}$$

It should be noted that only a linear solution is needed for added resistance computation, since the mean value of the second-order solution goes to zero; therefore, there is no need to solve a complete second-order boundary value problem. Details of this formula are presented in Juncquez (2009).

3.2.2. The far-field method (momentum conservation method)

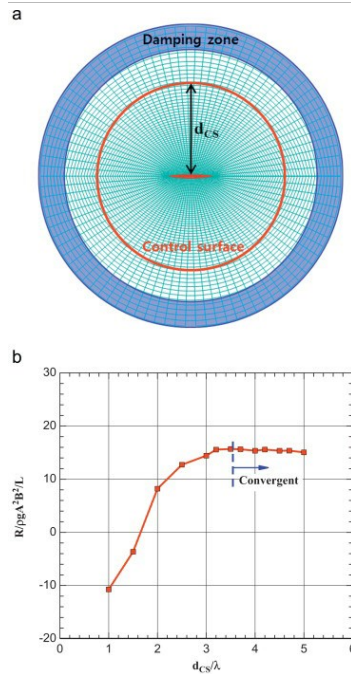
The mathematical background of the momentum conservation method is to consider a control volume around a ship hull, and then to derive a momentum balance. The second-order force can be obtained by calculating changing values of second-order momentum at the control surface of far-field. Under the assumption that there is one incoming wave, and the magnitude of velocity potential exponentially decreases with respect to the z-axis, the second-order force can be expressed as follows:

$$\begin{aligned} \vec{F}_2 &= \frac{1}{2} \rho \int_{C_p} \frac{(\nabla (\phi_1 + \phi_2) \cdot \nabla (\phi_1 + \phi_2) + k^2 (\phi_1 + \phi_2)^2)}{2k} \cdot \vec{n}_1 \cdot dL - \rho \int_{C_p} \frac{\nabla (\phi_1 + \phi_2) \cdot \nabla (\phi_1 + \phi_2)}{2k} \cdot dL \\ &\quad - \frac{1}{2} \rho \int_{C_p} (\zeta_1 + \zeta_2)^2 \vec{n}_1 \cdot dL - \rho \\ &\quad f_{C_p} [\nabla \Phi (\phi_1 + \phi_2) \cdot \vec{n}_1] + \nabla (\phi_1 + \phi_2) \cdot \nabla \Phi \cdot \vec{n}_1] (\zeta_1 + \zeta_2) \cdot dL \quad (32) \end{aligned}$$

C_p and \vec{n}_1 are the intersection of the control surface at infinity with the z=0 plane, and the normal vector of the control surface, respectively. k is the wave number.

To calculate the added resistance using the momentum conservation method combined with the Rankine panel method, a control surface should be chosen at a certain location. Fig. 3(a) shows an example of a control surface. Two factors should be considered in determining the control surface. First, it is necessary to place a control surface far enough away from the hull, in order to avoid any evanescent mode waves passing through the control surface. Secondly, it needs to be taken into account that the control surface should not overlap with the wave damping zone, where radiated waves

are absorbed. Therefore, the control surface is placed at a sufficient distance from a ship to avoid evanescent mode waves, but within the inner region of the damping zone starting point, as shown in Fig. 3(a). The circular shape of the control surface is chosen for convenience of manipulation.



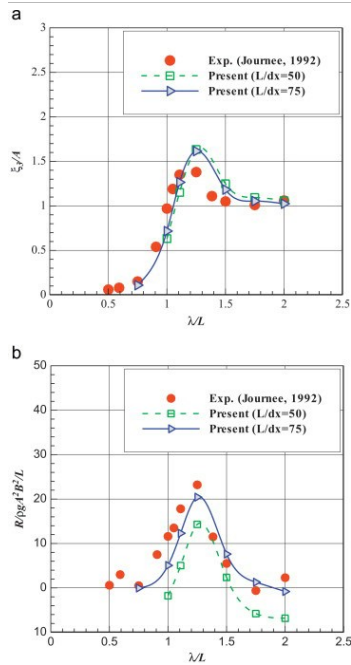
[Download : Download full-size image](#)

Fig. 3. Convergence test of a control surface: Wigley III, Fn=0.2, $\lambda/L=0.9$. (a) Example of control surface and (b) added resistance.

To confirm how far away a control surface should be located, the added resistances on a Wigley III hull are calculated with respect to the location of control surface. In Fig. 3(b), d_{CS} means the distance between the center of a model ship and the control surface, as shown in Fig. 3(a). As you can see in Fig. 3(b), if the control surface is placed farther than $d_{CS}/\lambda=3.0$, the added resistance converges to a certain value. This means that evanescent mode waves are fully decayed in this region. In general, the results of added resistance converge if the d_{CS}/λ is larger than 3.0; therefore, it is desirable to set the control surface at more than $d_{CS}/\lambda=3.0$.

3.3. The Cartesian grid method

In the Cartesian grid method, the added resistance is calculated by direct pressure integration. Steady problems are solved beforehand for each forward speed, with only fixed surge motion. Subtracting the steady surge force from the mean surge force, which is obtained from the motion problem, provides the added resistance. Fig. 4 shows the grid dependency test for a Wigley III hull with Fn=0.3. Only the results of different x -direction grid sizes are presented, because the grid spacing of the other directions has less influence on the results. The added resistance is more sensitive to the grid system than to the motion response. Since the grid system affects the representation of solid body shape, the added resistance differs according to small changes of body shape. It is difficult to say that the result of added resistance at $L/dx=75$ converges; however, the limitations of the grid system, such as aspect ratio and computational resource, mean that it is hard to use more grid. These values, therefore, are used in the added resistance results, which are presented in the following sections.



[Download : Download full-size image](#)

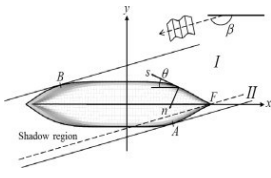
Fig. 4. Grid dependency of motion, and added resistance: Wigley III, Fn=0.3. (a) Heave motion RAO and (b) added resistance.

3.4. Added resistance in short waves

In short wavelengths, it is difficult to calculate added resistance accurately using the previous far- and near-field method, because the hydrodynamic nonlinear effects are intensified at the bow diffraction wave. To overcome this difficulty, a few researches have been carried out. Faltinsen et al. (1980) derived the asymptotic formula of added resistance in short waves. They assumed that the ship has vertical sides at the water plane, and that the wavelength is small compared to the draft of the ship. Due to the small wavelength assumptions, the influence of the wave-induced motions can be neglected, and it is only the part of the ship close to the water plane that will affect the flow field. From this, the following asymptotic formula can be derived.

$$R = \frac{1}{2} \rho g C_f^2 \int_0^\pi \left[\sin^2(\theta - \beta) + \frac{2\alpha_L}{\eta} \left[1 + \cos \theta \cos(\theta - \beta) \right] \right] \vec{n} \cdot dL n_1 = \sin \theta n_2 \\ = \cos \theta n_3 = x_0 \cos \theta - y_0 \sin \theta \quad (33)$$

where, θ is the waterline inclined angle, and β is the wave incident angle defined in Fig. 5. The integration in Eq. (33) is performed over the non-shaded part (A-F-B) of the waterline (Fig. 5).



[Download](#) : [Download full-size image](#)

Fig. 5. Coordinate system for the added resistance calculation in the short wave range (Faltinsen et al., 1980).

Fujii and Takahashi (1975) derived the semi-empirical formula of added resistance in short waves, by adopting some complement coefficients to the drifting force formula of a fixed vertical cylinder. Kuroda et al. (2008) proposed an improved expression based on Fujii and Takahashi's (1975) method, by modifying compliment coefficients. These two formulas can be expressed as follows:

$$R = \alpha_U(1 + \alpha_U) \left[\frac{1}{2} \rho g C_f^2 B B_f(\beta) \right] \quad (34)$$

$$B_f(\beta) = \frac{1}{\eta} \left[f_I \sin^2(\theta - \beta) \sin \theta d\theta + f_{II} \sin^2(\theta + \beta) \sin \theta d\theta \right] \quad \text{Fujii and Takahashi (1975)} \\ \text{Kuroda et al. (2008)} \alpha_U = \frac{\pi^2 I_1(k_e)}{\pi^2 (I_1(k_e) + K_1(k_e))} \quad \alpha_d = \frac{\pi^2 K_1(k_e)}{\pi^2 (I_1(k_e) + K_1(k_e))} \\ \left(k_e = \frac{\omega}{\eta} \right) 1 + \alpha_U = 1 + 5\sqrt{k_e} \\ 1 + \alpha_U = 1 + C_U F_u, \quad (C_U = \max[10.0, -310 B_f(\beta) + 68]) \quad (35)$$

These formulas comprise B_f the bluntness coefficient; α_d the reflection coefficient composed of ship draft and wave number; and $1+\alpha_U$ the advance speed coefficient. The integration is performed over two parts, I and II , which mean the non-shade port part and starboard part, respectively. I_1 and K_1 represent the modified Bessel function of the first kind of order 1, and modified Bessel function of the second kind of order 1, respectively. In the method of Kuroda et al. (2008), the advance speed coefficient and the reflection coefficient are modified. A regression coefficient, C_U , which is decided using experimental data, is proposed in the advance speed coefficient. Also, the encounter wave number k_e is substituted for the wave number k in the reflection coefficient, α_d . This means that the effect of advance speed is added not only to the advance speed coefficient, $1+\alpha_U$, but also to the reflection coefficient, α_d .

4. Numerical results

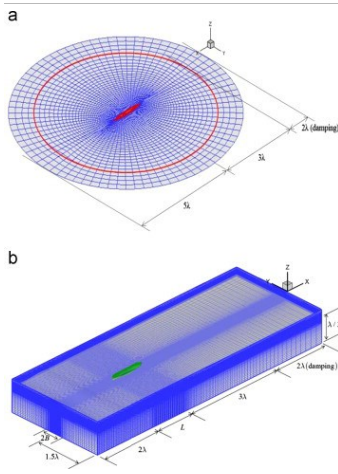
4.1. Test models

In order to verify and validate the developed program, several test models are considered: the Wigley I and III hulls, the Series 60 with block coefficients of 0.7 and 0.8, and the S175 containership. The main particulars of the test models are summarized in Table 1. The present computation starts from validation of the motion response, since motion response is a crucial part in added resistance. To this end, the computed motion responses of test ships are compared with the experimental data, and the added resistances on ships are then observed in regular waves.

Table 1. Principal particulars of test models.

Model	Wigley I	Wigley III	Series 60 $C_B=0.7$	Series 60 $C_B=0.8$	S175 containership
L (m)	100.0	100.0	100.0	121.92	175.0
B (m)	10.0	10.0	14.28	18.76	25.4
D (m)	6.25	6.25	5.7	7.5	9.5
C_B	0.560	0.462	0.7	0.8	0.561

In the solution panels of the Rankine panel method, as shown in Fig. 6(a), about 4000 panels are applied for a half domain. Fig. 6(b) shows a typical grid system used in the Cartesian grid method. Even though the number of grids depends on the wavelength and wave amplitude, the average number of grids is about 4 million to 5 million (280x130x130). Most of them are clustered near the ship and free-surface region.



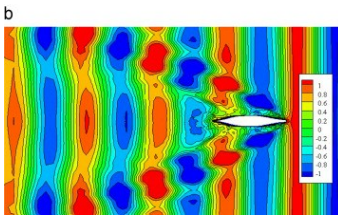
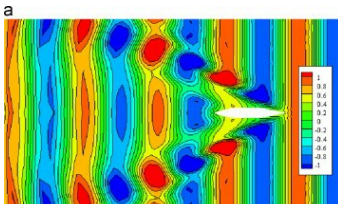
[Download](#) : [Download full-size image](#)

Fig. 6. Examples of solution grid: S175 containership. (a) Panel model for the Rankine panel method and (b) Grid distribution for the Cartesian grid method.

4.2. Motion response in a regular wave

The ship motion response is directly related to added resistance, especially the radiation component of added resistance. The exact calculation of the ship motion response, therefore, is important in accurately predicting the added resistance. Validation of the ship motion response is carried out in this section. In the present study, the frequency-domain strip method, time-domain Rankine panel method and Cartesian grid method are applied to analyze the ship motion problem. To validate the ship motion responses, heave and pitch motions calculated by each methods are compared with the experimental data.

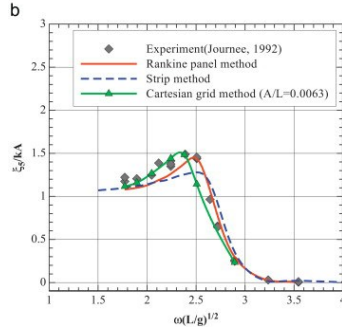
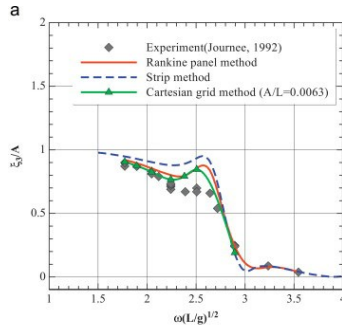
Fig. 7 shows the wave patterns around a S175 containership, calculated by the Rankine panel method and the Cartesian grid method. The overall tendency of the wave contour is similar; however, waves near the ship of the Cartesian grid method are more complicated than those of the Rankine panel method, since the Cartesian grid method provides a fully nonlinear solution.



[Download](#) : [Download full-size image](#)

Fig. 7. Wave contours around S175 containership: $F_n=0.2$, $\lambda/L=1.0$, $\beta=180^\circ$ (a) Rankine panel method and (b) Cartesian grid method.

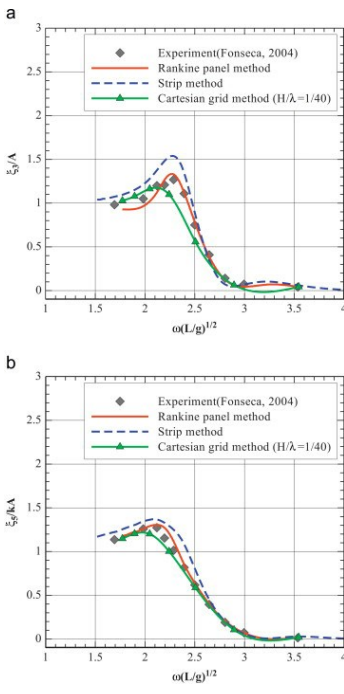
Fig. 8 shows the vertical motion responses of the Wigley III model at $F_n=0.2$. It should be mentioned that the wave amplitude in the Cartesian grid method is the same as the experimental condition. As shown in these figures, overall tendencies of the motion responses are similar to each other, and show good agreement with experimental data; however, small differences among computational results are shown, especially in the peak value frequency. In the strip method, the peak value frequency is slightly moved to the high frequency region, because the effect of ship speed cannot be exactly accounted for. In the Cartesian grid method, the peak frequency is slightly shifted to the low frequency region. The wavelength and wave amplitude are different between in waves and in calm water; thus, when the ship motion problem with forward speed is solved, there is a limitation in providing sufficient mesh resolution to capture all the information, especially the steady components.



[Download](#) : [Download full-size image](#)

Fig. 8. Comparison of vertical motions: Wigley III, $F_n=0.2$, $\beta=180^\circ$ (a) Heave motion RAO and (b) Pitch motion RAO.

Fig. 9 shows the heave and pitch motion RAOs of a S175 containership at $F_n=0.25$. The Rankine panel method and Cartesian grid method give similar vertical motions, and agree well with measured data; while the strip method gives a slightly greater magnitude of heave motion than the experimental data.



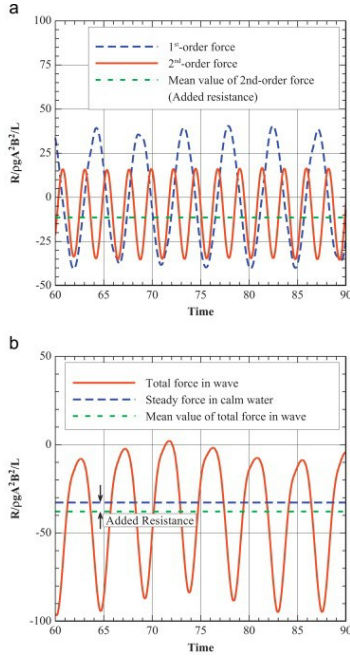
[Download : Download full-size image](#)

Fig. 9. Comparison of vertical motions: S175 containership, $F_n=0.25$, $\beta=180^\circ$ (a) Heave motion RAO and (b) Pitch motion RAO.

4.3. Added resistance in regular waves

To compare the capability and accuracy of the prediction of added resistance between the developed programs, the computational results of added resistances on Wigley hull models, Series 60 ($C_B=0.7$, 0.8) and a S175 containership are compared with the experimental data. Only the Wigley III hull and the S175 containership cases are considered in the Cartesian grid method.

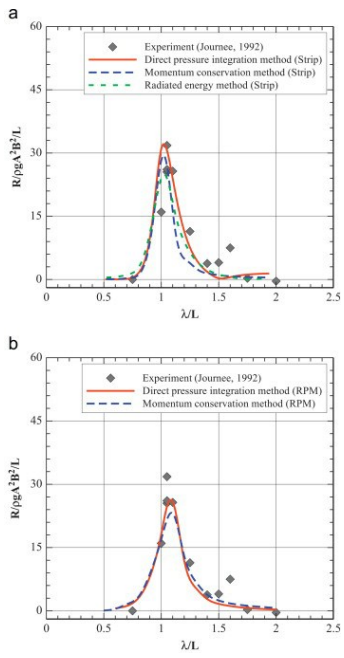
Fig. 10 shows the time signals of surge forces on the Wigley III model with $F_n=0.3$. Fig. 10(a) and (b) represent the time histories of the far-field method applied to the Rankine panel method and the Cartesian grid method, respectively. In Fig. 10(a), linear- and second-order forces are shown, and the second-order force contains only the quadratic components of linear solutions, as presented in Eq. (32). Naturally, the second-order force oscillates two times faster than the linear force. In Fig. 10(b), the total force in waves and steady force in calm water are shown. The added resistance is predicted by the difference between mean values of the total force in waves and steady force in calm water.



[Download : Download full-size image](#)

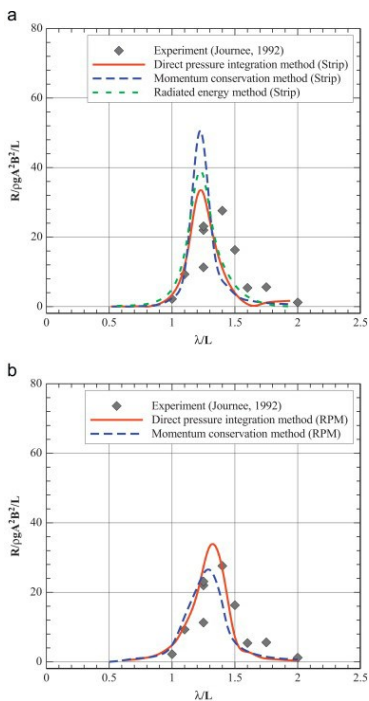
Fig. 10. Time signals of surge force on Wigley III model: $F_n=0.3$, $\lambda/L=1.0$, $\beta=180^\circ$ (a) Rankine panel method and far-field method and (b) Cartesian grid method.

Fig. 11, Fig. 12 show the results of added resistance on the Wigley I model with respect to wavelength in a head sea in $F_n=0.2$ and 0.3, respectively. All computations are carried out in a regular wave. R represents the averaged second-order force of the longitudinal component, i.e. $-r_{xz}$. In Fig. 11, Fig. 12 (a) is the computational results of added resistance computed by the strip method and (b) is the computational results of added resistance computed by the Rankine panel method. In Fig. 11, the low forward speed case, there is no remarkable difference among the calculation results, and the computational results show favorable agreements with the experimental data. Fig. 12 shows the added resistance on the ship when the ship speed is relatively large ($F_n=0.3$). As shown in this figure, discrepancies among the numerical results are shown, especially in the peak value frequency. The peak value frequency of the strip method is located at the short wave region.



[Download : Download full-size image](#)

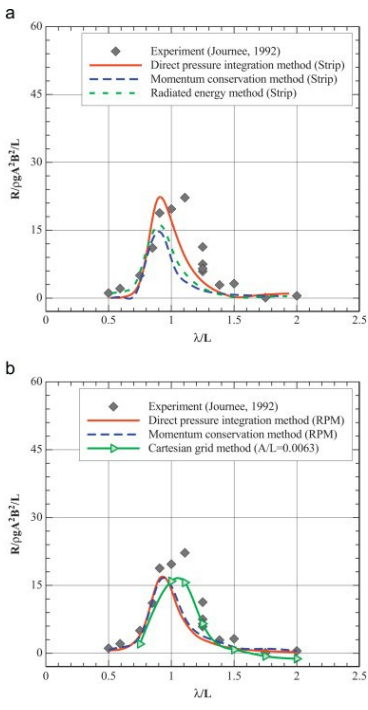
Fig. 11. Comparison of added resistance on Wigley I model: $F_n=0.2$, $\beta=180^\circ$ (a) Strip method and (b) Rankine panel method.



[Download : Download full-size image](#)

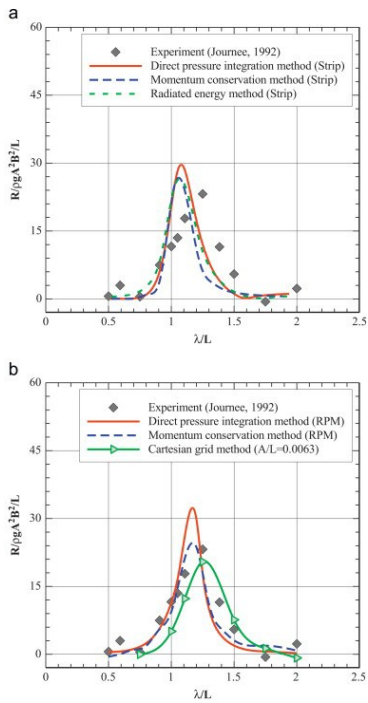
Fig. 12. Comparison of added resistance on Wigley I model: $F_n=0.3$, $\beta=180^\circ$ (a) Strip method and (a) (b) Rankine panel method.

Fig. 13, Fig. 14 show the added resistances on a Wigley III model with $F_n=0.2$ and 0.3 , respectively. In the case of $F_n=0.2$, all of the computational methods give similar values to each other; however the magnitudes of added resistance are lower than the experimental data near $\lambda/L=1.2$ (peak value frequency of experimental data). The Wigley III model is more slender than the Wigley I model, which means that the disturbance of the Wigley III model is smaller than that of the Wigley I model. Because it is difficult to capture a small amount of disturbance, added resistance on the Wigley III model shows relatively poorer correspondence with the experimental data, than that on the Wigley I model at $F_n=0.2$. In the case of $F_n=0.3$, there is a slight discrepancy among the computational results; peak value frequencies computed by the strip methods are located at the short wave range, and the magnitude of added resistance calculated by the Cartesian grid method in short wavelength is small, compared to the experimental data. These tendencies are similar to the motion response. This means that the motion response crucially affects the prediction of added resistance. The results of the Rankine panel method show better agreement with the experimental data, than those of the other methods.



[Download](#) : [Download full-size image](#)

Fig. 13. Comparison of added resistance on Wigley III model: $Fn=0.2$, $\beta=180^\circ$ (a) Strip method and (b) Rankine panel method and Cartesian grid method.

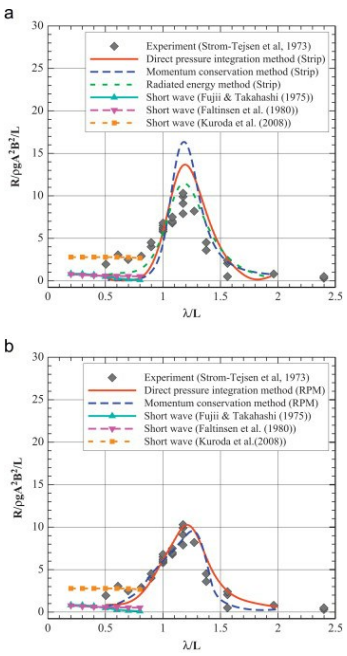


[Download](#) : [Download full-size image](#)

Fig. 14. Comparison of added resistance on Wigley III model: $Fn=0.3$, $\beta=180^\circ$ (a) Strip method and (b) Rankine panel method and Cartesian grid method.

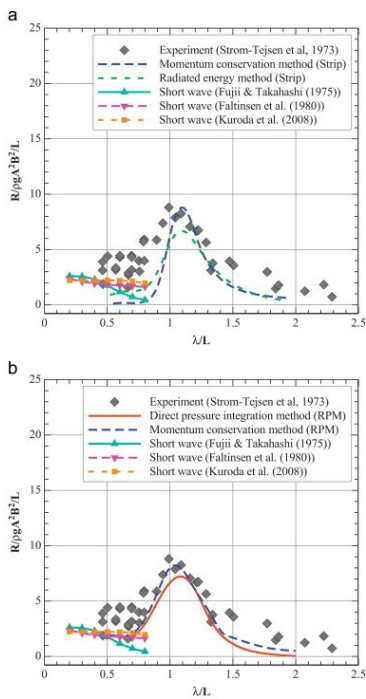
As shown in Fig. 11, Fig. 12, Fig. 13, Fig. 14, the computational results show reasonable agreements with the experimental data at a low Froude number, while they show small discrepancies compared to the measured data at a high Froude number, especially in the prediction of peak value frequency. In these cases, the strip methods give a less accurate peak value frequency than the other methods. If the ship moves faster, the encounter frequency is larger, and the peak value frequency of added resistance moves into the longer wave range. The strip method, however, cannot exactly account for the effect of ship speed. It seems that this causes the slight discrepancy in the peak value frequency between the strip method and the experimental data. In the case of the difference between the results of the Rankine panel method, the result of the direct pressure integration method and that of the momentum conservation method must theoretically be the same, from the viewpoint of momentum conservation; however, small differences are in fact shown. These differences come from the limitation of exact numerical implementation. For instance, to calculate the added resistance using the momentum conservation method, values on a free-surface panel that is far enough from the ship are used, instead of exact far-field values. These cause small differences between the two methods.

The added resistance of Series 60 ($C_B=0.7$) with $Fn=0.222$, and that of Series 60 ($C_B=0.8$) with $Fn=0.15$, are shown in Fig. 15, Fig. 16. In Fig. 15, the momentum conservation method combined with the Rankine panel method gives better agreement with the experimental data, than do other methods. In Fig. 16, the added resistance calculated by the strip method shows a poor correspondence with the experimental data, compared to the results of the Rankine panel method. In this case, while the Froude number is not that high, the block coefficient is relatively large, which cause the poor results of the strip methods. In the case of short wave calculation, all methods show good correspondence with the experimental data for Series 60 $C_B=0.8$; however, only Kuroda et al. (2008) method gives good agreement with the experimental data for Series 60 $C_B=0.7$. It was already mentioned that Fujii and Takahashi's (1975) and Faltinsen et al. (1980) methods give good agreements with experimental data for relatively blunt bodies, while some poor agreements are obtained for fine hulls. Kuroda et al. (2008) method, however, gives good agreements for fine hulls too, because they supplemented their formula using experimental data.



[Download : Download full-size image](#)

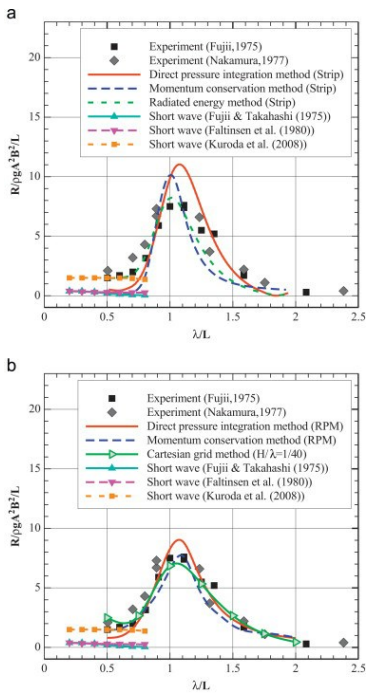
Fig. 15. Comparison of added resistance on Series 60 $C_B=0.7$ model: $Fn=0.222$, $\beta=180^\circ$ (a) Strip method and (b) Rankine panel method.



[Download : Download full-size image](#)

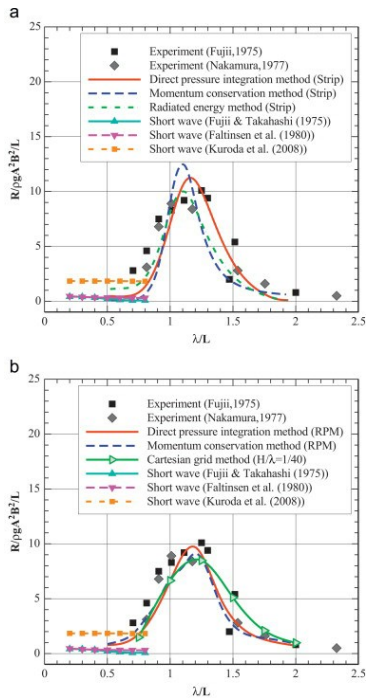
Fig. 16. Comparison of added resistance on Series 60 $C_B=0.8$ model: $Fn=0.15$, $\beta=180^\circ$ (a) Strip method and (b) Rankine panel method.

Added resistance on an S175 containership is shown in Fig. 17, Fig. 18. In these figures, a similar tendency can be observed. As the Froude number increases, the discrepancies among the results of the numerical methods increase. Generally, the results calculated by the Cartesian grid method show better correspondences with experimental data than do those of the other methods. In the case of short wave calculations, the method of Kuroda et al. (2008) predicts the added resistance better than do other approximation formulae. Because the S175 containership has a relatively fine hull, only Kuroda et al. (2008) method gives good correspondence with the experimental data.



[Download : Download full-size image](#)

Fig. 17. Comparison of added resistance on S175: $Fn=0.20$, $\beta=180^\circ$ (a) Strip method and (b) Rankine panel method and Cartesian grid method.

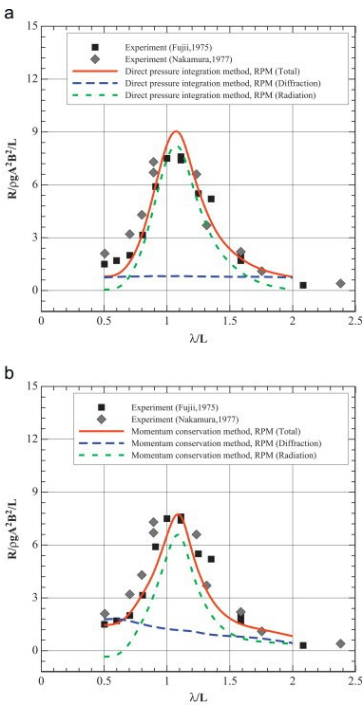


[Download : Download full-size image](#)

Fig. 18. Comparison of added resistance on S175: $Fn=0.25$, $\beta=180^\circ$. (a) Strip method and (b) Rankine panel method and Cartesian grid method.

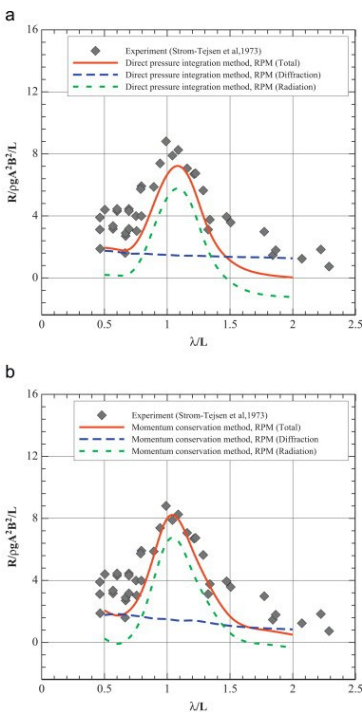
4.4. Component decomposition

Added resistance can be composed of two components; the radiation and diffraction component. Fig. 19, Fig. 20 show the radiation and diffraction component of added resistance on a S175 containership and a Series 60 $C_B=0.8$, respectively. In these figures, (a) and (b) represent the added resistance components calculated by the direct pressure integration method and by the momentum conservation method combined with the Rankine panel method. As you can see in these figures, the radiation component is much larger than the diffraction component in the near resonance wavelength. The diffraction component does not vary significantly with respect to the wavelength, while the radiation component dramatically changes, depending on the wavelength. In short waves, the diffraction component is larger than the radiation component in both methods.



[Download : Download full-size image](#)

Fig. 19. Component of added resistance on S175 computed by the Rankine panel method: Fn=0.20, $\beta=180^\circ$. (a) Near-field method and (b) far-field method.



[Download : Download full-size image](#)

Fig. 20. Component of added resistance on Series 60 $C_B=0.8$ computed by the Rankine panel method: Fn=0.15, $\beta=180^\circ$ (a) Near-field method and (b) far-field method.

5. Conclusions

In this study, three different numerical methods are used to predict the added resistance on a ship: the strip method, Rankine panel method, and Cartesian-grid method. In the case of the strip method and Rankine panel method, the far- and near-field approaches are applied to solve the added resistance problem. In the case of the Cartesian grid method, the added resistance is calculated by subtracting the steady surge force from the mean surge force, measured in waves. In addition, to complement the results of added resistance in short wavelengths, the established asymptotic calculation methods are examined. Computational results are validated by comparing them with experimental data on the Wigley hulls, the Series 60 hulls, and the S175 container ship models, and show reasonable agreements. From this study, the following conclusions can be made:

- In the case of motion response, the vertical motion response shows small differences among calculation results, especially in the peak value frequency. The frequency of the peak value in the strip method is slightly moved to the high frequency region, and the peak frequency of the Cartesian grid method is slightly shifted to the low frequency region. These tendencies are shown in the added resistance results. This means that the motion response crucially affects the prediction of added resistance.
- In the low speed case, the results of added resistance calculated by all methods are similar, and agree well with the experimental data, while in the high speed case, small discrepancies among the numerical results are shown. In particular, the peak value frequency of the strip method is slightly shifted to the short wave region compared to the experimental data, because the effect of the ship speed cannot be exactly accounted for.
- Generally, the added resistances calculated by strip methods show reasonable correspondence with the experimental data except for short waves. However, some discrepancy can be observed when the ship speed is high, and the ship hull is a relatively blunt body. Therefore, the strip method is a good practical tool for the calculation of added resistance when the bow shape is not blunt and the ship speed is not very high if an appropriate approximation method is combined for short wave range.

- According to the present case of added resistance in short waves, all methods ([Fujii and Takahashi, 1975](#), [Faltinsen et al., 1980](#), [Kuroda et al., 2008](#)) give reasonable agreements with experimental data for a relatively blunt body, while only the method of [Kuroda et al. \(2008\)](#) gives reasonable results for a slender ship. This implies it is necessary to choose a proper method with respect to the shape of the ship.
- The added resistance quantities are generally larger in strip method than three-dimensional methods. According to our computational experience, the overall performance of three-dimensional methods is better than strip method, particularly in short wave regions. Furthermore, it is clear that the 3D methods predict better agreement in the prediction of frequency of peak added resistance.

Acknowledgment

This study has been partly supported by the Korean Ministry of Knowledge Economy (MKE), project number [10040030](#), and also partly supported by the LRF*-Funded Research Center at Seoul National University. Their support is greatly appreciated. The administrative support of RIMSE and ERI are also acknowledged. (* Lloyd's Register Foundation(LRF): a UK registered charity and sole shareholder of Lloyd's Register Group Ltd., invests in science, engineering and technology for public benefit, worldwide)

[Recommended articles](#) [Citing articles \(58\)](#)

References

- Bærentzen and Aanæs, 2005** J.A. Bærentzen, H. Aanæs
Signed distance computation using the angle weighted pseudonormal
 IEEE Transactions on Visualization and Computer Graphics, 11 (3) (2005), pp. 243-253
[View Record in Scopus](#) [Google Scholar](#)
- Bunnik et al., 2010** Bunnik, T., Daalen, E. van Kapsenberg, G., Shin, Y., Huijsmans, R., Deng, G., Delhommeau, G., Kashiwagi, M., Beck, B., 2010. A comparative study on state-of-the-art prediction tools for seakeeping. In: Proceedings of the 28th Symposium on Naval Hydrodynamics. California, USA, pp. 1-13.
[Google Scholar](#)
- Eberly, 2008** Eberly, D., 2008. Distance between point and triangle in 3D (Online). Available from: <<http://www.geometricstools.com>>.
[Google Scholar](#)
- Faltinsen et al., 1980** Faltinsen, O.M., Minsaas, K.J., Liapis, N., Skjørdal, S.O., 1980. Prediction of resistance and propulsion of a ship in a seaway. In: Proceedings of the 13th Symposium on Naval Hydrodynamics. Tokyo, Japan, pp. 505-529.
[Google Scholar](#)
- Fang and Chen, 2006** M.C. Fang, G.R. Chen
On the nonlinear hydrodynamic forces for a ship advancing in waves
 Ocean Engineering, 33 (2006), pp. 2119-2134
[Article](#) [Download PDF](#) [View Record in Scopus](#) [Google Scholar](#)
- Fujii and Takahashi, 1975** Fujii, H., Takahashi, T., 1975. Experimental study on the resistance increase of a ship in regular oblique waves. In: Proceedings of the 14th International Towing Tank Conference. Ottawa, Canada, pp. 351-360.
[Google Scholar](#)
- Gerritsma and Beukelman, 1972** J. Gerritsma, W. Beukelman
Analysis of the resistance increase in waves of a fast cargo ship
 International Shipbuilding Progress, 19 (217) (1972), pp. 285-293
[CrossRef](#) [View Record in Scopus](#) [Google Scholar](#)
- Grue and Biber, 1993** J. Grue, D. Biber
Wave forces on marine structures with small speed in water of restricted depth
 Applied Ocean Research, 15 (1993), pp. 121-135
[Article](#) [Download PDF](#) [CrossRef](#) [View Record in Scopus](#) [Google Scholar](#)
- Hu and Kashiwagi, 2004** C. Hu, M. Kashiwagi
A CIP-based method for numerical simulations of violent free-surface flows
 Journal of Marine Science and Technology, 9 (2004), pp. 143-157
[CrossRef](#) [View Record in Scopus](#) [Google Scholar](#)
- Hu and Kashiwagi, 2007** Hu, C., Kashiwagi, M., 2007. Numerical and experimental studies on three-dimensional water on deck with a modified wigley model. In: Proceedings of the 9th International Conference on Numerical Ship Hydrodynamics. Michigan.
[Google Scholar](#)
- Joncquez et al., 2008** Joncquez, S.A.G., Bingham, H., Andersen, P., 2008. Validation of added resistance computations by a potential flow boundary element method. In: Proceedings of the 27th Symposium on Naval Hydrodynamics. Seoul, Korea, pp. 1461-1470.
[Google Scholar](#)
- Joncquez, 2009** Joncquez, S.A.G. 2009. Second-Order Forces and Moments Acting on Ships in Waves (Ph.D. thesis). Technical University of Denmark, Copenhagen, Denmark.
[Google Scholar](#)
- Joosen, 1966** Joosen, W.P.A., 1966. Added resistance of ships in waves. In: Proceedings of the 6th Symposium on Naval Hydrodynamics. Washington, D.C.
[Google Scholar](#)
- Journee, 1992** Journee, J.M.J., 1992. Experiments and calculations on four Wigley hull forms. Delft University of Technology Report.
[Google Scholar](#)
- Kashiwagi et al., 2009** Kashiwagi, M., Takehiro, I., Takuma, S., 2009. Effect of forward speed of a ship on added resistance in waves. In: Proceedings of the 19th International Conference on Offshore and Polar Engineering. Osaka, Japan, pp. 818-825.
[Google Scholar](#)
- Kim and Kim, 2011** K.H. Kim, Y. Kim
Numerical study on added resistance of ships by using a time-domain Rankine panel method
 Ocean Engineering, 38 (2011), pp. 1357-1367
[Article](#) [Download PDF](#) [View Record in Scopus](#) [Google Scholar](#)
- Kim et al., 2012** K.H. Kim, M.K. Seo, Y. Kim
Numerical analysis on added resistance of ships
 International Society of Offshore and Polar Engineers, 21 (1) (2012), pp. 21-29
[View Record in Scopus](#) [Google Scholar](#)
- Kim et al., 2010** Kim, Y., Kim, K.H., Kim, J.H., Kim, T.Y., Seo, M.G., Kim, Y., 2010. Time-domain analysis of nonlinear motion responses and structural loads on ships and offshore structures: development of WISH programs. In: Proceedings of the ITTC Workshop on Seakeeping. Seoul, Korea, pp. 19-21.
[Google Scholar](#)
- Kuroda et al., 2008** M. Kuroda, M. Tsujimoto, T. Fujiwara, S. Ohmatsu, K. Takagi
Investigation on Components of Added Resistance in Short Waves
 Journal of the Japan Society of Naval Architects and Ocean Engineers, 8 (2008), pp. 171-176
[CrossRef](#) [View Record in Scopus](#) [Google Scholar](#)
- Liu et al., 2011** S. Liu, A. Papanikolaou, G. Zaraphonitis
Prediction of added resistance of ships in waves
 Ocean Engineering, 38 (2011), pp. 641-650

Maruo, 1960 H. Maruo

The drift of a body floating on waves

Journal of Ship Research, 4 (3) (1960), pp. 1-10

[View Record in Scopus](#) [Google Scholar](#)

Nakamura and Naito, 1977 S. Nakamura, S. Naito

Propulsive performance of a containership in waves

Journal of the Society of Naval Architects of Japan, 15 (1977), pp. 24-48

[View Record in Scopus](#) [Google Scholar](#)

Nakos, 1990 Nakos, D.E., 1990. Ship Wave Patterns and Motions by a Three Dimensional Rankine Panel Method (Ph.D. thesis). MIT, Cambridge, USA.

[Google Scholar](#)

Newman, 1967 J.N. Newman

The Drift Force and Moment on Ships in Waves

Journal of Ship Research, 11 (1967), pp. 51-60

[CrossRef](#) [View Record in Scopus](#) [Google Scholar](#)

Orihara and Miyata, 2003 H. Orihara, H. Miyata

Evaluation of added resistance in regular incident waves by computational fluid dynamics motion simulation using an overlapping grid system

Journal of Marine Science and Technology, 8 (2003), pp. 47-60

[View Record in Scopus](#) [Google Scholar](#)

Salvesen et al., 1970 N. Salvesen, E.O. Tuck, O.M. Faltinsen

Ship Motions and Sea Loads

Transactions of the Society of Naval Architects and Marine Engineers, 78 (1970), pp. 250-279

[Google Scholar](#)

Salvesen 1978 Salvesen, N., 1978. Added resistance of ship in waves. Journal of Hydraulics 12(1), 24-34.

[Google Scholar](#)

Sclavounos, 1985 Sclavounos, P.D., 1985. User's Manual of NIIRID. MIT Report.

[Google Scholar](#)

Storm-Tejsen et al., 1973 J. Storm-Tejsen, H.Y.H. Yeh, D.D. Moran

Added resistance in waves

Transactions of the Society of Naval Architects and Marine Engineers, 81 (1973), pp. 250-279

[Google Scholar](#)

Waterson and Deconinck, 2007 N.P. Waterson, H. Deconinck

Design principles for bounded higher-order convection schemes—a unified approach

Journal of Computational Physics, 224 (2007), pp. 182-207

[Article](#) [Download PDF](#) [View Record in Scopus](#) [Google Scholar](#)

Xiao et al., 2005 F. Xiao, Y. Honma, T. Kono

A simple algebraic interface capturing scheme using hyperbolic tangent function

International Journal for Numerical Methods in Fluids, 48 (2005), pp. 1023-1040

[CrossRef](#) [View Record in Scopus](#) [Google Scholar](#)

Ye and Hsiung, 1997 H.K. Ye, C.C. Hsiung

Computation of added wave resistance of a restrained floating body in the time-domain.

International Shipbuilding Progress, 44 (437) (1997), pp. 25-57

[Google Scholar](#)

Yokoi, 2007 K. Yokoi

Efficient Implementation of THINC scheme: a simple and practical smoothed VOF algorithm

Journal of Computational Physics, 226 (2007), pp. 1985-2002

[Article](#) [Download PDF](#) [View Record in Scopus](#) [Google Scholar](#)

[View Abstract](#)



About ScienceDirect

Remote access

Shopping cart

Advertise

Contact and support

Terms and conditions

Privacy policy

We use cookies to help provide and enhance our service and tailor content and ads. By continuing you agree to the [use of cookies](#).

Copyright © 2021 Elsevier B.V. or its licensors or contributors. ScienceDirect® is a registered trademark of Elsevier B.V.

ScienceDirect® is a registered trademark of Elsevier B.V.

RELX™

FEEDBACK